Supporting Information for

Self-Assembly of Sequence-Regulated Amphiphilic Copolymers with Alternating Rod and Coil Pendants

Weisheng Feng, Liquan Wang,* Shaoliang Lin*

Shanghai Key Laboratory of Advanced Polymeric Materials, Key Laboratory for Ultrafine Materials

of Ministry of Education, Frontiers Science Center for Materiobiology and Dynamic Chemistry,

School of Materials Science and Engineering, East China University of Science and Technology,

Shanghai 200237, China

*E-mail: lq_wang@ecust.edu.cn; slin@ecust.edu.cn

1. Simulation Method

Dissipative particle dynamics (DPD) is a coarse-grained mesoscopic simulation approach, which was first introduced by Hoogerbrugge and Koelman and improved by Espa$\tilde{n}$ol and Warren.[1] In the DPD model, each bead represents a cluster of atoms or molecules. The movement of DPD beads obeys Newton's equation of motion,

$$\frac{\mathrm{d}\mathbf{r}_i}{\mathrm{d}t} = \mathbf{v}_i, \quad m\frac{\mathrm{d}\mathbf{v}_i}{\mathrm{d}t} = \mathbf{f}_i \tag{S1}$$

where $\mathbf{r}_i$, $\mathbf{v}_i$, $\mathbf{f}_i$, and m are the position, velocity, total force, and mass of the ith bead, respectively. The total force $\mathbf{f}_i$ exerted on the ith bead is the sum of a conservative force $\mathbf{F}_{ij}^{\mathrm{C}}$, a dissipative force $\mathbf{F}_{ij}^{\mathrm{D}}$, a random force $\mathbf{F}_{ij}^{\mathrm{R}}$, and a bonding force $\mathbf{F}_{ij}^{\mathrm{S}}$, given by

$$\mathbf{f}_i = \sum_{j \neq i} \left(\mathbf{F}_{ij}^{\mathrm{C}} + \mathbf{F}_{ij}^{\mathrm{D}} + \mathbf{F}_{ij}^{\mathrm{R}} + \mathbf{F}_{ij}^{\mathrm{S}} \right) \tag{S2}$$

The conservative force is a soft repulsion for nonbonded beads,

$$\mathbf{F}_{ij}^{\mathrm{C}} = a_{ij}\sqrt{\omega^{\mathrm{C}}\left(r_{ij}\right)}\hat{\mathbf{r}}_{ij} \tag{S3}$$

where a_{ij} is the maximum repulsive interaction between the ith and jth beads; $\mathbf{r}_{ij} = \mathbf{r}_i - \mathbf{r}_j$; $r_{ij} = \left|\mathbf{r}_{ij}\right|$; $\hat{\mathbf{r}}_{ij} = \mathbf{r}_{ij}/r_{ij}$. The weight function $\omega^{\mathrm{C}}\left(r_{ij}\right)$ is given by

$$\omega^{\mathrm{C}}\left(r_{ij}\right) = \begin{cases} \left(1 - r_{ij}/r_{\mathrm{c}}\right)^2, & \left(r_{ij} < r_{\mathrm{c}}\right) \\ 0, & \left(r_{ij} > r_{\mathrm{c}}\right) \end{cases} \tag{S4}$$

where $r_{\mathrm{c}} = 1$ is the cutoff radius. The dissipative force, a friction force acting on the relative velocities of the beads, is

$$\mathbf{F}_{ij}^{\mathrm{D}} = -\gamma\omega^{\mathrm{D}}\left(r_{ij}\right)\left(\hat{\mathbf{r}}_{ij} \cdot \mathbf{v}_{ij}\right)\hat{\mathbf{r}}_{ij} \tag{S5}$$

where $\mathbf{v}_{ij} = \mathbf{v}_i - \mathbf{v}_j$; γ is the friction coefficient; $\omega^{\mathrm{D}}\left(r_{ij}\right)$ is weight functions describing the range of dissipative. The random force compensates the loss of kinetic energy due to the dissipative force, is

given as

$$\mathbf{F}_{ij}^{R} = \mu\omega^{R}\left(r_{ij}\right)\Gamma_{ij}\Delta t^{-1/2}\hat{\mathbf{r}}_{ij}$$ (S6)

where μ is the noise amplitude; $\omega^{R}\left(r_{ij}\right)$ is random forces vanishing at $r = r_{c}$, respectively. Γ_{ij} is a randomly fluctuating variable with Gaussian statistics, satisfies

$$\left\langle\Gamma_{ij}\left(t\right)\right\rangle = 0, \ \left\langle\Gamma_{ij}\left(t\right)\Gamma_{kl}\left(t'\right)\right\rangle = \left(\delta_{ik}\delta_{jl} + \delta_{il}\delta_{jk}\right)\delta\left(t - t'\right)$$ (S7)

Only one of $\omega^{D}\left(r_{ij}\right)$ or $\omega^{R}\left(r_{ij}\right)$ can be chosen arbitrarily to satisfy the fluctuation-dissipation theorem and the equilibrium Gibbs-Boltzman distribution. They are determined by the relation as follows.

$$\omega^{D}\left(r_{ij}\right) = \left[\omega^{R}\left(r_{ij}\right)\right]^{2} = \omega^{C}\left(r_{ij}\right)$$ (S8)

The values of parameters γ and μ are coupled by

$$\mu^{2} = 2\gamma k_{B}T\Delta t$$ (S9)

where T is the absolute temperature and k_{B} is the Boltzmann constant. Here, $k_{B}T$ and γ are chosen to be 1.0 and 4.5, respectively.

For the polymer system, the interaction force between bonded beads is described by a harmonic spring force,

$$\mathbf{F}_{ij}^{S} = k_{S}\left(1 - r_{ij}/r_{eq}\right)\hat{\mathbf{r}}_{ij}$$ (S10)

where k_{S} is the spring constant, and r_{eq} is the bond equilibrium length. We chose $k_{S} = 50$ and $r_{eq} = 0.86$. The angle force is added between every two consecutive bonds to guarantee the rigidity of rigid blocks. The angle force $\mathbf{F}^{A}$ is given by

$$\mathbf{F}^{A} = -\nabla\left[k_{A}\left(\pi - \theta\right)^{2}\right]$$ (S11)

where k_{A} is the angle constant and θ is the bond angle. The k_{A} was set to 40 to ensure the rigidity of rod blocks. In the DPD method, reduced units are adopted for all physical quantities, including the

cutoff radius r_c, the bead mass m, and the temperature $k_B T$. The time unit τ can be formulated by

$$\tau = \sqrt{mr_c^2 / k_B T} \tag{S12}$$

2. Simulation snapshots of morphologies

Fig. S1 shows simulation snapshots of the entire simulation box (excluding solvent) for each self-assembly morphology. As shown in Fig. S1a, the onion-like vesicle is a vesicle with two layers of rigid beads and a solvent-containing center. The cylindrical vesicle is a cylindrical structure with solvent in the middle (Fig. S1b). The spherical vesicles have one layer of rigid beads and a solvent-containing center (Fig. S1c). Cylindrical micelle (Fig. S1d) and spherical micelles (Fig. S1e) are common in self-assembly. The disk-like micelle is an aggregate in which all the hydrophobic beads are localized on a disk with coil chains uniformly distributed on the surface (Fig. S1f and Fig. S2). The lamellae percolating the simulation box can be regarded as perforated lamellae (Fig. S1g). The tube is a cylindrical vesicle of infinite length (Fig. S1h). The bowl-like micelle is disk-like micelles with a concave center (Fig. S1i).
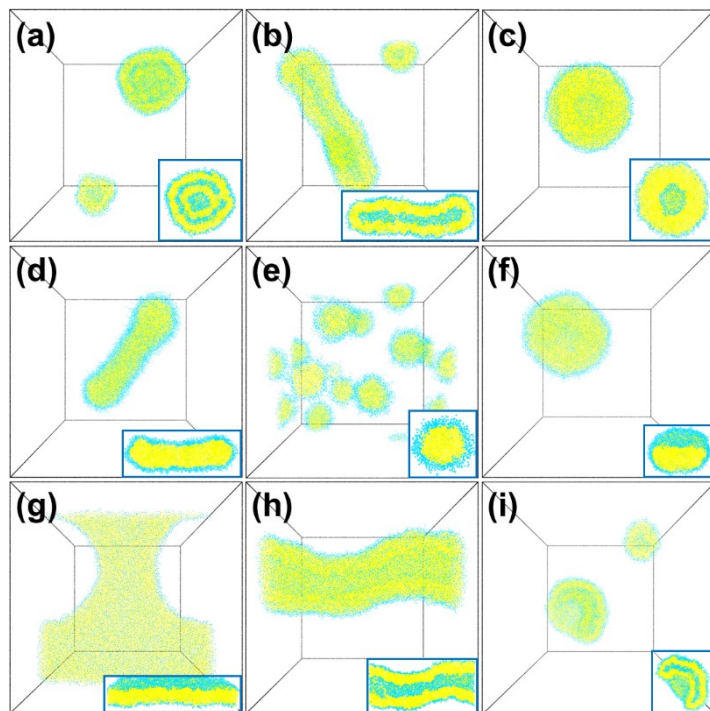
Fig. S1 Simulation snapshots of the entire simulation box (excluding solvent) for each of self-assembly morphologies. (a) onion-like vesicles ((C_1-*alt*-R_3)$_6$, 5%), (b) cylindrical vesicles ((C_1-*alt*-R_4)$_6$, 5%), (c) spherical vesicles ((C_1-*alt*-R_8)$_6$, 5%), (d) cylindrical micelles ((C_5-*alt*-R_8)$_6$, 5%), (e) spherical micelles ((C_5-*alt*-R_4)$_6$, 5%), (f) disk-like micelles ((C_3-*alt*-R_9)$_6$, 5%), (g) lamellae ((C_1-*alt*-R_7)$_6$, 10%), (h) tubes ((C_1-*alt*-R_9)$_3$, 10%), and (i) bowl-like micelles ((C_1-*alt*-R_3)$_6$, 5%). The insets show the cross-sections of such morphologies.
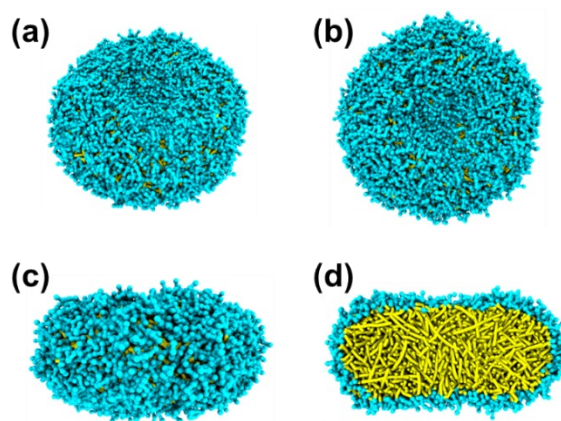
Fig. S2 (a) Snapshots, (b) top view, (c) front view, and (d) section of disk-like micelles formed by (C_3-*alt*-R_9)$_6$.

## 3. Five independent simulation results of onion-like vesicles

Fig. S3 shows five independent simulation results of $(C_1\text{-}alt\text{-}R_3)_6$. As shown, although there are several aggregates in each simulated box, onion-like vesicles are the predominant structures. The results for other morphologies are similar, which means that the results of the five replicate simulations end up in the same phase.
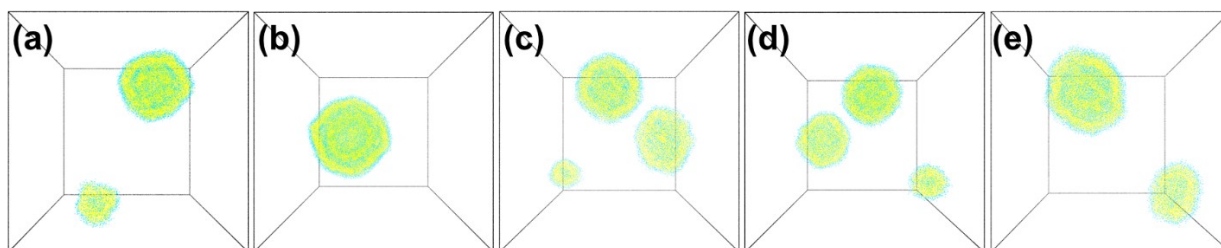
Fig. S3 Five independent simulation results of $(C_1\text{-}alt\text{-}R_3)_6$, where the copolymer concentration is 5%.

# 4. Simulation results of onion-like vesicles at extended times

Fig. S4 shows the snapshots of $(C_1\text{-}alt\text{-}R_3)_6$ at extended simulation times. As shown, the aggregate morphology did not change with increasing the simulation time, which means that the onion-like vesicles are stable.
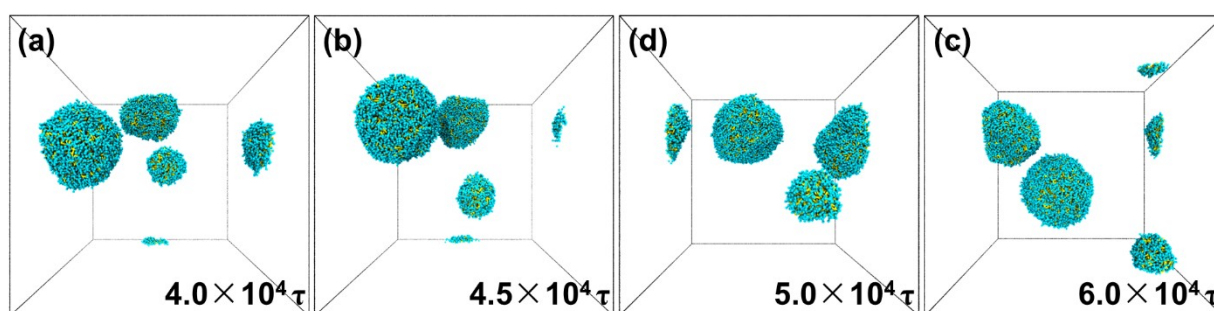
Fig. S4 Simulation snapshots of onion-like vesicles formed by $(C_1\text{-}alt\text{-}R_3)_6$ at extended simulation times.

5. Evolution of Surface Areas for Different Replicates

Fig. S5 shows the time evolution (after 20000τ for clarity) of the surface areas of the other four replicates formed by $(C_1\text{-}alt\text{-}R_3)_6$, where the copolymer concentration is 5%. As shown, the time of each stage of these replicates may be different, but the variations are basically consistent.
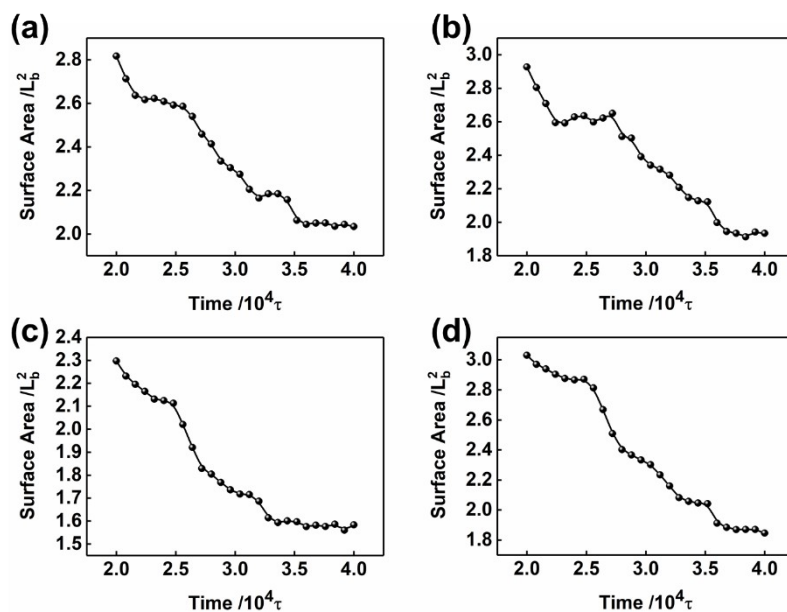
Fig. S5 Time evolution of the surface areas of four replicates formed by $(C_1\text{-}alt\text{-}R_3)_6$, where the copolymer concentration is 5%. The unit L_b on the vertical coordinate is the length of the simulation box.

6. Orientational Arrangement of Rod Pedants

We used the order parameter S to evaluate the orientational arrangement of rod blocks in self-assembled aggregates. The order parameter S is defined as[S2]

$$S_i = \frac{3(\mathbf{u}_i \cdot \mathbf{u}_d)^2 - 1}{2} \qquad (S13)$$

where $\mathbf{u}_i$ and $\mathbf{u}_d$ represent the normalized vector of the ith rod block and the director, respectively. The $\mathbf{u}_d$ is calculated by iteration to find the maximum value of $\sum_{i=1}^{N}(\mathbf{u}_i \cdot \mathbf{u}_d)^2$. However, traditional order parameters cannot reveal the collection of rigid chains in some structures, such as a vesicular wall.

The local order parameter, the average over the order parameter of every rigid chain with neighboring rigid chains, can describe the arrangement of rigid chains in a vesicular wall. As illustrated in Fig. S6, the neighboring domain is defined by a cylindrical domain centered at a rigid segment. The cylindrical domain possesses radius R and length L, where R and L are $2.0r_c$ and $4.0r_c$, respectively. The rigid segment with one or more beads located in this cylindrical domain is categorized as the neighboring rigid chain. This local order parameter derives from the short-range order parameter used in the study carried out by Sheng et al.[S3] In their research, the R and L were related to the length L_{rod} of rigid chains ($L = L_{rod}$ and $R = \frac{L_{rod}}{2\sqrt{3}}$). Because of the relatively small cylindrical area for short L_{rod}, we found that this short-range order parameter would result in an irrational increment with short rigid segments. Consequently, we fixed the value of R and L to obtain the local order parameter.
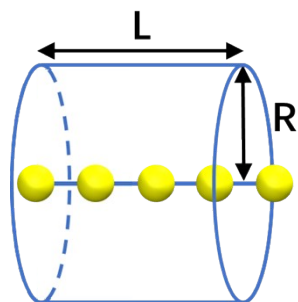
Fig. S6 Schematic of the neighboring cylindrical domain centered at a rigid chain.

7. Self-Assembly Induced by Rod-to-Coil Conformation Transition of Rigid Pendants

To realize the rod-to-coil conformation transition, we set the constant k_A of bond angle potential to be 0 to eliminate the rigidity of pendants and then performed another simulation with 1.0×10^6 DPD steps ($4.0 \times 10^4 \tau$) under this condition. Fig. S7 presents the morphological transformation from spherical micelles, disk-like micelles, and cylindrical micelles after the rod-to-coil conformation transition of rigid pendants. We observed a sphere-to-vesicle change induced by the rod-to-coil conformation transition for spherical micelles, as shown in Fig. S7a. As the angle forces in rigid pendants disappear, spherical micelles gather into disk-like micelles, which bend into vesicles. The disk-like micelles collapse with a noticeable reduction in thickness and finally forms vesicles (Fig. S7b). The cylindrical micelles first collapse into disk-like micelles, and the disk-like micelles concave and eventually form vesicles due to the edge effect (Fig. S7c). These results indicate that the vesicles are more stable assemblies after the rod-to-coil conformation transition.
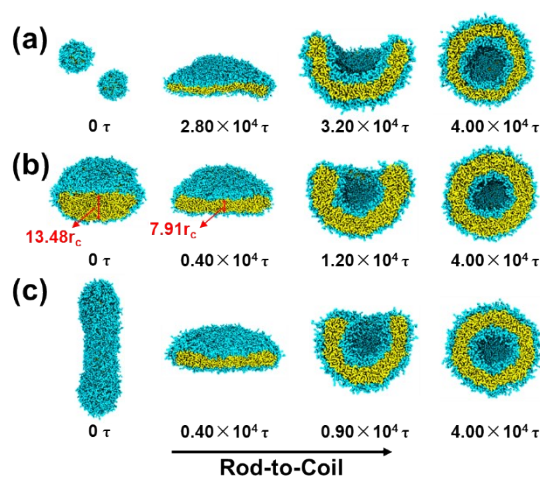
Fig. S7 Morphological transformations from (a) spherical micelles formed by $(C_4\text{-}alt\text{-}R_5)_6$, (b) disk-like micelles formed by $(C_3\text{-}alt\text{-}R_9)_6$, and (c) cylindrical micelles formed by $(C_5\text{-}alt\text{-}R_8)_6$ induced by the rod-to-coil conformation transition of rigid pendants, where the copolymer concentration is 5%.

8. Drug Loading Process of Spherical Micelles

We also simulated the process of loading one class of drugs. Firstly, the coil alternating copolymers $(C_7\text{-}alt\text{-}D_6)_6$ are assembled in solvents selective to the D pendents. Afterward, the drug M was added to the system at a lower concentration (5%) for further self-assembly. The drugs are slightly hydrophobic ($a_{MS} = 30$, $a_{MC} = 40$), and the interaction parameter between the drugs and D pendants is 27($a_{MR} = 27$). As shown in Figure S8, the alternating copolymer first self-assembles into spherical micelles. After the drug is added, the drug will enter the inside of the micelles because they are compatible with the D pendants.

C: Hydrophilic coil bead
D: Hydrophobic coil bead
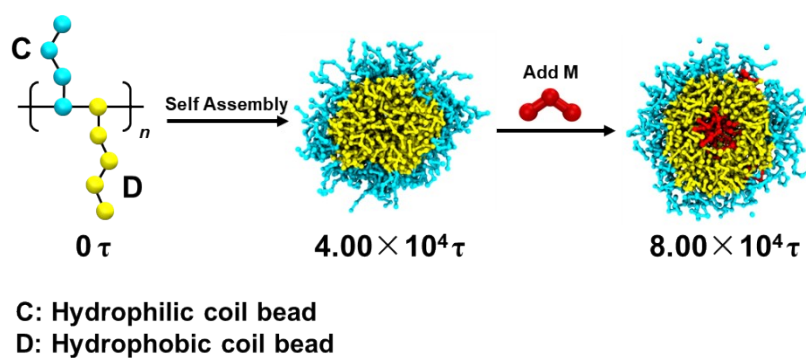
Fig. S8 Schematic representation of the spherical micelles drug loading process.

Reference

1 R. D. Groot and P. B. Warren, *J. Chem. Phys.*, 1997, **107**, 4423-4435.

2 Y. Lv, L. Wang, F. Wu, S. Gong, J. Wei and S. Lin, *Phys. Chem. Chem. Phys.*, 2019, **21**, 7645-7653.

3 S. H. Chou, H. K. Tsao and Y. J. Sheng, *J. Chem. Phys.*, 2011, **134**.